Tämä on rinnakkaistallenne. Rinnakkaistallenteen sivuasettelut ja typografiset yksityiskohdat saattavat poiketa alkuperäisestä julkaisusta.

Käytä viittauksessa alkuperäistä lähdettä:

Kullaa, J. (2020). Robust damage detection in the time domain using Bayesian virtual sensing with noise reduction and environmental effect elimination capabilities. *Journal of Sound and Vibration*, vol 473.

Special Issue at the occasion of the ISMA2018 International Noise and Vibration Conference

Robust damage detection in the time domain using Bayesian virtual sensing with noise reduction and environmental effect elimination capabilities

Jyrki Kullaa

Metropolia University of Applied Sciences, School of Automotive and Mechanical Engineering, P.O. Box 4071, 00079 Metropolia, Finland

ARTICLE INFO

ABSTRACT

Vibration-based structural health monitoring aims at detecting changes in the dynamic characteristics of a structure. A direct time-domain damage detection method is proposed, in which no system identification is needed. In this data-based method, response signals are acquired using a sensor network. Utilizing hardware redundancy, each sensor signal can be estimated from the remaining signals in the network. The residuals, or the differences between the actual and estimated signals are used for damage detection. However, the measurement error affects the detection performance. Therefore, a novel two-step algorithm is proposed. The signal-to-noise ratio of the signals is first increased by developing Bayesian virtual sensors that are proved to be more accurate than the hardware. Virtual sensor data then replace the actual measurements in the subsequent data analysis. In the second step, environmental or operational influences can be eliminated by acquiring training data under different conditions and estimating the signal of each sensor using the remaining virtual sensors in the network. The excitation or the environmental or operational variables are not measured. In this two-step algorithm for damage detection, each sensor's signal is estimated twice. The novelty is how to apply Bayesian virtual sensors to residual generation resulting in enhanced damage detection. Principal component analysis is applied to the residuals and an extreme value statistics control chart is designed for damage detection. Vibrations of a healthy and damaged bridge structure were simulated under random excitation and temperature variability. Virtual sensors outperformed the actual measurements in damage detection making an early warning more plausible.

© 2020 Elsevier Ltd. All rights reserved.

1. Introduction

Structural health monitoring (SHM) can replace visual inspections of important infrastructure. Several nondestructive techniques are available for damage detection, for example radiographic testing, thermography, ultrasonic testing, vibration-based methods, acoustic emission, electromagnetic testing, and optical methods [1]. Vibration-based methods are attractive, because damage can be detected remotely from the sensor. In vibration-based SHM, a large sensor network is installed on the structure and changes in the dynamic characteristics of the structure are an indication of structural deterioration. Traditionally, the dynamic characteristics are the natural frequencies, mode shapes, or damping of the structure, extracted from the

vibration measurements. An alternative is to perform the data analysis directly in the time domain. In order to make the monitoring system reliable, an early warning (detection of minor damage) and a small number of false alarms are necessary.

A complimentary approach is to build a numerical model of the system using, for example, the finite element method. The model is then updated to correspond the measurement data using optimization techniques, which results in a better approximation of the physical system. Damage identification is also based on model updating, in which the model parameters indicate the location and severity of damage. Model updating is an inverse method, for which optimization techniques are often used. Recent studies include different optimization methods to identify damage in a composite laminate [2], locate cracks in plate structures [3,4] and in beam-like structures [5], update a model of a bridge with a comparison of different joint models [6], detect damage using a Cornwell damage indicator [2], a modified Cornwell damage indicator [7], or a normalized strain energy indicator [8], and enhance training of artificial neural network to find a global minimum for damage identification [9]. In many of the aforementioned studies isogeometric analysis method has been used instead of the more traditional finite element method [2–4,8].

In order to make SHM competitive, the following issues must be solved.

1. Measurement error. The desired level of damage to be detected is relatively small, which means that the signal-to-noise ratio must be high.
2. Environmental or operational influences are often stronger than those of damage, which can make damage detection difficult.
3. The excitation cannot be measured or controlled. The data analysis method must be based on response data only.
4. The data analysis must be automatic due to a vast amount of data.
5. In physics-based SHM, an accurate finite element model is needed, which may cause additional costs and challenges.
6. A large sensor network is needed with simultaneous sampling of all channels.

This paper concentrates on a time-domain data analysis for damage detection and localization. The aforementioned issues are discussed in a more detail in the following.

First, the signal-to-noise-ratio (SNR) of the measured signals can be increased using virtual sensing techniques. The SNR should be maximised for optimal detection performance [10]. The main contribution of this paper is noise reduction using empirical Bayesian virtual sensing [11]. Different empirical virtual sensing techniques have been applied to sensor validation and sensor fault identification [12–24]. In a redundant sensor network, it is possible to estimate the signal of each sensor using the other sensors in the network. However, it is not guaranteed that the estimated signal is more accurate than the original signal. In the present study, Bayes' rule is applied to the sensor network resulting in optimal weights for the reconstruction of each signal. The accuracy of the Bayesian virtual sensors is always higher than that of the actual sensors. Virtual sensing is applied independently to each measurement. Consequently, the variability between the measurements (environmental or operational influences or changes due to damage) remains. Virtual sensor data then replace the actual measurements in the subsequent data analysis.

Second, environmental or operational variability affects the dynamic behaviour of the structure. For civil engineering structures, the main underlying variable is temperature [25–30], but also the influences of the water level in the dam [31], humidity on a wooden structure [32], traffic [33,34], and wind [35] have been identified.

Because the underlying environmental or operational variables are not all known and their effects on the data are often complex, it may be difficult to build a model that predicts the variability in the data. An alternative is to apply multivariate statistical techniques to the response data only. Due to the environmental or operational variability, the measured variables become correlated, which can be utilized to remove the underlying influences from the data.

Many techniques have been developed to compensate for the environmental or operational effects without a need to measure the underlying variables [32,36–50]. The conditional probability is used in this paper using the minimum mean square error (MMSE) estimation [51]. The same technique can be used either in the time-domain [24] or in the feature-domain [48]. Training data are needed from the undamaged structure under different environmental and operational conditions.

Third, damage detection must be performed using output-only data. Two main concerns in the time-domain methods are the amplitude and frequency of the excitation. It is assumed that the structure is linear and the response can be expressed with sufficient accuracy by including only a few lowest modes. This is often a valid assumption with civil engineering structures under low-frequency ambient excitation. The amplitude of the excitation has a direct effect on the SNR. Therefore, larger amplitudes should be preferred. If the response is very small, the noise floor may mask the relevant information in the measured signal. Notice that a stationary process assumption is not needed in the proposed method.

Fourth, because of a time-domain approach, system identification is not needed, which makes the data analysis much easier to automate. The proposed method is indeed fully automatic. The data covariance matrix is only needed for the residual generation.

Fifth, a data-based algorithm for damage detection and localization is used, and no finite element model is needed.

Finally, a large sensor network is needed both to localize damage to the nearest sensor and to make the measurement system redundant. The redundancy is needed to decrease the measurement error and to eliminate the environmental or operational influences. A large number of sensors increases the hardware and maintenance costs (e.g. sensors, cables, data

acquisition, data storage, assembly, and repair). A wireless sensor network (WSN) is a possible solution with a large number of low-cost sensor nodes and automatic reconfiguration. Time synchronization in a WSN is an issue, because simultaneous sampling is required. Also, low-cost sensors may be less accurate than the more traditional high-quality sensors. An optical measurement system is also an alternative to acquire response measurements from a large number of channels. Sensor technology is, however, beyond the scope of this study and is not discussed any further in this paper.

In this paper a direct time-domain damage detection method is proposed, which is based on a novel two-step algorithm. In the first step, Bayesian virtual sensors are estimated separately for each measurement in order to reduce the measurement error. The objective of the second step is residual generation for damage detection. The training data are acquired under different conditions and used to estimate the signal of each sensor using the remaining virtual sensors in the network. In this two-step algorithm, each sensor's signal is estimated twice. The novelty is how to apply Bayesian virtual sensors to residual generation resulting in enhanced damage detection.

The paper is organized as follows. Bayesian virtual sensors are derived in Section 2. Damage detection under varying environmental or operational conditions is outlined in Section 3. Detection and localization of a crack in a bridge girder is studied in Section 4 using a numerical finite element model to generate vibration measurements under different environmental and operational effects. Concluding remarks are given in Section 5.

2. Bayesian virtual sensing

Virtual sensing (VS) gives an estimate of a quantity of interest using the available measurements. Empirical VS is a data-based approach, estimating a physical sensor using hardware redundancy. The sensor might become faulty, and using historical data from the functioning sensor network, the sensor reading can be reconstructed. Analytical VS utilizes a mathematical model together with measurements to estimate a quantity of interest. For example, full-field data can be estimated using a limited number of sensors.

This study applies empirical VS to noisy measurements to estimate less noisy virtual sensors. Bayes' rule is applied to a sensor network, and it is shown that the posterior is more accurate than the actual hardware. The derivation of Bayesian virtual sensors is reviewed based on [11] and applied to damage identification.

2.1. Bayes' rule

Consider a sensor network measuring p simultaneously sampled variables $\mathbf{y} = \mathbf{y}(t)$ at time t. Each measurement $\mathbf{y}$ includes independent measurement error $\mathbf{w} = \mathbf{w}(t)$:

$$\mathbf{y} = \mathbf{x} + \mathbf{w} \tag{1}$$

where $\mathbf{x} = \mathbf{x}(t)$ are the true values of the measured degrees of freedom (DOFs). The objective is to find a less noisy estimate for the true values $\mathbf{x}$ utilizing the noisy measurements $\mathbf{y}$ from the sensor network.

The signals of a subset of the physical sensors is estimated by partitioning each observation into observed variables $\mathbf{v}$ and estimated variables $\mathbf{u}$ (typically a single sensor u). The partitioned variables are

$$\mathbf{y} = \left\{ \begin{array}{c} \mathbf{y}_u \\ \mathbf{y}_v \end{array} \right\}, \quad \mathbf{x} = \left\{ \begin{array}{c} \mathbf{x}_u \\ \mathbf{x}_v \end{array} \right\}, \quad \mathbf{w} = \left\{ \begin{array}{c} \mathbf{w}_u \\ \mathbf{w}_v \end{array} \right\} \tag{2}$$

The measurement error $\mathbf{w}$ is assumed to be zero mean, independent of $\mathbf{x}$, with a known covariance matrix

$$\mathbf{\Sigma}_w = \mathrm{E}\left(\mathbf{w}\mathbf{w}^T \right) = \begin{bmatrix} \mathbf{\Sigma}_{w,uu} & \mathbf{\Sigma}_{w,uv} \\ \mathbf{\Sigma}_{w,vu} & \mathbf{\Sigma}_{w,vv} \end{bmatrix} \tag{3}$$

where $\mathrm{E}(\cdot)$ denotes the expectation operator. After partitioning, all distributions are conditioned with $\mathbf{y}_v$. Bayes' rule becomes

$$
\begin{aligned}
p(\mathbf{x}_u|\mathbf{y}) &= p(\mathbf{x}_u|\mathbf{y}_u, \mathbf{y}_v) \\
&= \frac{p(\mathbf{y}_u|\mathbf{x}_u, \mathbf{y}_v)p(\mathbf{x}_u|\mathbf{y}_v)}{p(\mathbf{y}_u|\mathbf{y}_v)} \\
&= \frac{p(\mathbf{y}_u|\mathbf{x}_u)p(\mathbf{x}_u|\mathbf{y}_v)}{p(\mathbf{y}_u|\mathbf{y}_v)}
\end{aligned}
\tag{4}
$$

The distributions in Eq. (4) can be evaluated as shown in the following.

2.2. Likelihood

Assuming Gaussian noise $\mathbf{w}$, the likelihood is obtained using Eq. (1):

$$p(\mathbf{y}_u|\mathbf{x}_u) = N(\mathbf{y}_u|\mathbf{x}_u, \mathbf{\Sigma}_{w,uu})$$

$$\propto \exp\left[-\frac{1}{2}(\mathbf{y}_u - \mathbf{x}_u)^T\mathbf{\Sigma}_{w,uu}^{-1}(\mathbf{y}_u - \mathbf{x}_u)\right] \tag{5}$$

2.3. Evidence

For simplicity but without loss of generality, assume zero-mean variables $\mathbf{y}$. The partitioned data covariance matrix $\mathbf{\Sigma}_y$ is

$$\mathbf{\Sigma}_y = \mathrm{E}\left(\mathbf{y}\mathbf{y}^T\right) = \begin{bmatrix} \mathbf{\Sigma}_{y,uu} & \mathbf{\Sigma}_{y,uv} \\ \mathbf{\Sigma}_{y,vu} & \mathbf{\Sigma}_{y,vv} \end{bmatrix} \tag{6}$$

The precision matrix $\mathbf{\Gamma}_y$ is defined as the inverse of the covariance matrix $\mathbf{\Sigma}_y$ and is also written in a partitioned form:

$$\mathbf{\Gamma}_y = \mathbf{\Sigma}_y^{-1} = \begin{bmatrix} \mathbf{\Gamma}_{y,uu} & \mathbf{\Gamma}_{y,uv} \\ \mathbf{\Gamma}_{y,vu} & \mathbf{\Gamma}_{y,vv} \end{bmatrix} \tag{7}$$

A linear minimum mean square error (LMMSE) estimate for $\mathbf{y}_u | \mathbf{y}_v$ is obtained by minimizing the mean-square error (MSE) and can be computed either using the covariance or precision matrix [23,52]. If each sensor signal is estimated in turn, the formulas based on the precision matrix result in a more efficient algorithm [23]. The expected value of the estimated variable is:

$$\widehat{\mathbf{y}}_u = \mathrm{E}(\mathbf{y}_u|\mathbf{y}_v) = -\mathbf{\Gamma}_{y,uu}^{-1}\mathbf{\Gamma}_{y,uv}\mathbf{y}_v = \mathbf{K}\mathbf{y}_v \tag{8}$$

where $\mathbf{K} = -\mathbf{\Gamma}_{y,uu}^{-1}\mathbf{\Gamma}_{y,uv}$, and the error covariance is

$$\mathrm{cov}(\mathbf{y}_u|\mathbf{y}_v) = \mathbf{\Gamma}_{y,uu}^{-1} \tag{9}$$

The evidence $p(\mathbf{y}_u|\mathbf{y}_v)$ is also Gaussian with the mean and covariance from Eqs. (8) and (9), respectively:

$$p\left(\mathbf{y}_u|\mathbf{y}_v\right) = N(\mathbf{y}_u|\mathbf{K}\mathbf{y}_v, \mathbf{\Gamma}_{y,uu}^{-1})$$

$$\propto \exp\left[-\frac{1}{2}(\mathbf{y}_u - \mathbf{K}\mathbf{y}_v)^T\mathbf{\Gamma}_{y,uu}(\mathbf{y}_u - \mathbf{K}\mathbf{y}_v)\right] \tag{10}$$

The evidence is merely a normalizing factor, independent of $\mathbf{x}_u$. However, the evidence will be utilized in damage detection to remove the environmental or operational effects, which will be discussed in Section 3.

2.4. Prior

The prior distribution $p(\mathbf{x}_u|\mathbf{y}_v)$ is obtained from the measurement model, Eq. (1), by partitioning and conditioning, and applying the rule that the sum of two Gaussian variables is also a Gaussian variable. The prior mean is

$$\mathrm{E}(\mathbf{x}_u|\mathbf{y}_v) = \mathrm{E}(\mathbf{y}_u|\mathbf{y}_v) - \mathrm{E}(\mathbf{w}_u) = \mathrm{E}(\mathbf{y}_u|\mathbf{y}_v) = \mathbf{K}\mathbf{y}_v \tag{11}$$

and the prior covariance is obtained from

$$\mathrm{cov}(\mathbf{y}_u|\mathbf{y}_v) = \mathrm{cov}(\mathbf{x}_u|\mathbf{y}_v) + \mathbf{\Sigma}_{w,uu} \tag{12}$$

from which and Eq. (9),

$$\mathbf{\Sigma}_{\mathrm{prior},uu} = \mathrm{cov}(\mathbf{x}_u|\mathbf{y}_v)$$

$$= \mathrm{cov}(\mathbf{y}_u|\mathbf{y}_v) - \mathbf{\Sigma}_{w,uu} = \mathbf{\Gamma}_{y,uu}^{-1} - \mathbf{\Sigma}_{w,uu} \tag{13}$$

The prior distribution is also Gaussian:

$$p(\mathbf{x}_u|\mathbf{y}_v) = N(\mathbf{x}_u|\mathbf{K}\mathbf{y}_v, \boldsymbol{\Sigma}_{\text{prior},uu})$$
$$\propto \exp\left[-\frac{1}{2}(\mathbf{x}_u - \mathbf{K}\mathbf{y}_v)^T \boldsymbol{\Sigma}_{\text{prior},uu}^{-1}(\mathbf{x}_u - \mathbf{K}\mathbf{y}_v)\right] \tag{14}$$

Notice that the prior is not subjective. It is the distribution of the exact quantity, estimated without using the corresponding sensor signal.

2.5. Posterior

The posterior distribution, Eq. (4), is obtained by some manipulation, resulting in

$$
\begin{aligned}
p(\mathbf{x}_u|\mathbf{y}) &= c_1 p(\mathbf{y}_u|\mathbf{x})p(\mathbf{x}_u|\mathbf{y}_v) \\
&= c_2 \exp\left[-\frac{1}{2}(\mathbf{y}_u - \mathbf{x}_u)^T \boldsymbol{\Sigma}_{w,uu}^{-1}(\mathbf{y}_u - \mathbf{x}_u) - \frac{1}{2}(\mathbf{x}_u - \mathbf{K}\mathbf{y}_v)^T \boldsymbol{\Sigma}_{\text{prior},uu}^{-1}(\mathbf{x}_u - \mathbf{K}\mathbf{y}_v)\right] \\
&= c_3 \exp\left[-\frac{1}{2}\left(\mathbf{x}_u - \widehat{\mathbf{x}}_u\right)^T \boldsymbol{\Sigma}_{\text{post},uu}^{-1}\left(\mathbf{x}_u - \widehat{\mathbf{x}}_u\right)\right]
\end{aligned}
\tag{15}
$$

where c_1, c_2, and c_3 are constants and the posterior covariance $\boldsymbol{\Sigma}_{\text{post},uu}$ is

$$\boldsymbol{\Sigma}_{\text{post},uu} = \text{cov}(\mathbf{x}_u|\mathbf{y}) = \left(\boldsymbol{\Sigma}_{w,uu}^{-1} + \boldsymbol{\Sigma}_{\text{prior},uu}^{-1}\right)^{-1} \tag{16}$$

and the posterior mean is

$$\widehat{\mathbf{x}}_u = E(\mathbf{x}_u|\mathbf{y}) = \boldsymbol{\Sigma}_{\text{post},uu}\left(\boldsymbol{\Sigma}_{w,uu}^{-1}\mathbf{y}_u + \boldsymbol{\Sigma}_{\text{prior},uu}^{-1}\mathbf{K}\mathbf{y}_v\right) \tag{17}$$

A block diagram is shown in Fig. 1, in which sensor 1 is estimated using a total number of p sensors. Notice that the MSE of the posterior, Eq. (16), is always smaller than that of the measurement error, $\boldsymbol{\Sigma}_{w,uu}$. Therefore, the posterior mean is more accurate than the actual measurement.

Eq. (17) can also be written in the following form.

$$\widehat{\mathbf{x}}_u = \left[\boldsymbol{\Sigma}_{\text{post},uu}\boldsymbol{\Sigma}_{w,uu}^{-1} \quad \boldsymbol{\Sigma}_{\text{post},uu}\boldsymbol{\Sigma}_{\text{prior},uu}^{-1}\mathbf{K}\right]\begin{Bmatrix}\mathbf{y}_u \\ \mathbf{y}_v\end{Bmatrix} = \mathbf{a}_u^T\mathbf{y} \tag{18}$$
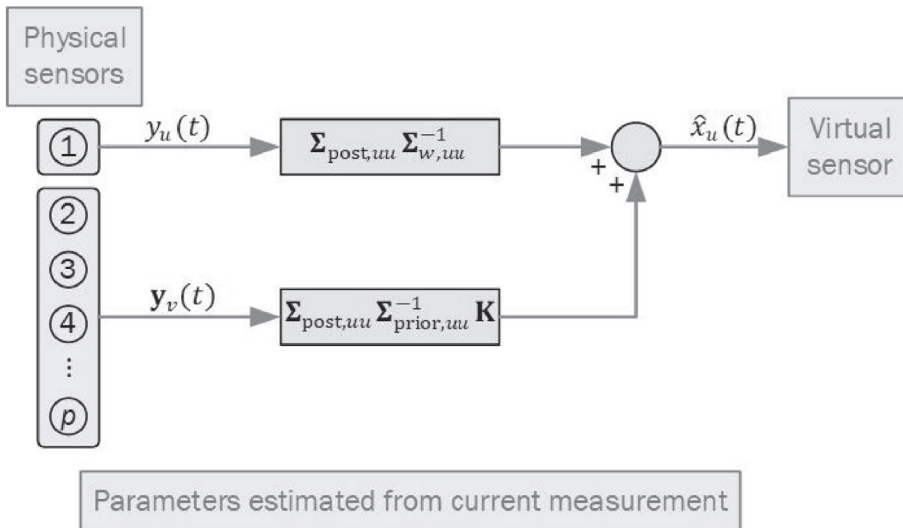
where $\mathbf{a}_u^T$ is

Fig. 1. A block diagram of Bayesian virtual sensing (17) of sensor 1 in a sensor network with p sensors.

$$\mathbf{a}_u^T = \left[\; \mathbf{\Sigma}_{\text{post},uu} \mathbf{\Sigma}_{w,uu}^{-1} \quad \mathbf{\Sigma}_{\text{post},uu} \mathbf{\Sigma}_{\text{prior},uu}^{-1} \mathbf{K} \; \right] \tag{19}$$

Eq. (18) shows that the posterior mean is a weighted sum of the measurements of all sensors in the network.

Generally, the predicted DOFs **u** may include several variables. In the sequel, **u** is one-dimensional including one sensor only. For each sensor u, a corresponding row vector $\mathbf{a}_u^T$ is computed. All these vectors can be assembled in a coefficient matrix **A** to estimate all virtual sensors simultaneously:

$$\hat{\mathbf{x}} = \mathbf{A}\mathbf{y} \tag{20}$$

where each row u of matrix **A** represents the corresponding sensor.

2.6. Application of virtual sensing

Bayesian virtual sensing is applied to each measurement separately (Fig. 1). It is assumed that a single measurement is acquired under a constant environmental or operational condition, so that the dynamic characteristics remain the same during the whole measurement period. Because the measurement period is typically of the order of a few seconds or minutes, this assumption is often valid. Therefore, the differences between measurements due to environmental or operational variability or damage remain in the data. The noise is only reduced. The virtual sensors are then used for damage detection as shown in the following.

3. Damage detection under different environmental or operational conditions

Virtual sensors are used in damage detection as if they were physical hardware. The virtual sensor data replace the actual measurement data ($\mathbf{y} \leftarrow \hat{\mathbf{x}}$), Eq. (20). The damage detection algorithm used in this paper is briefly outlined. Each sensor in turn is estimated using the remaining sensors in the network. The residuals for each sensor are then generated:

$$\boldsymbol{\varepsilon}_u = \mathbf{y}_u - \mathrm{E}(\mathbf{y}_u | \mathbf{y}_v) \tag{21}$$

where $\mathbf{y}_u$ is a vector of virtual sensor data, Eq. (17) or (18) and $\mathrm{E}(\mathbf{y}_u | \mathbf{y}_v)$ is the evidence mean, Eq. (8), identified using training data (virtual sensors) from the undamaged structure. The training data consist of several measurements in order to take different environmental or operational conditions into account. Specifically, the data covariance matrix, Eq. (6), is estimated using all training data. The environmental or operational influences can be eliminated using correlation between the sensors, or more specifically the evidence mean [48]. Once damage occurs, the correlation structure does not fit the experimental data producing a larger residual, which will then trigger an alarm. A block diagram of residual generation of a single sensor in a sensor network including p sensors is shown in Fig. 2 when using a) physical or b) virtual sensors.

All residuals are standardized according to the training data. All samples, training and test data, are subjected to principal component analysis (PCA). The first principal component (PC) is retained in order to find the direction with the largest change
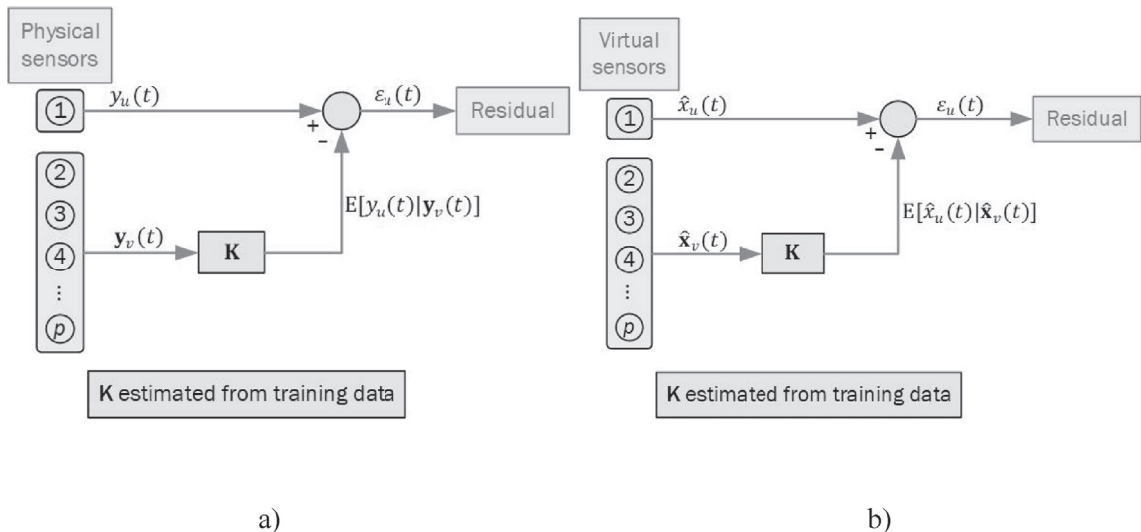

a)   b)

Fig. 2. A block diagram of residual generation (21) of sensor 1 in a sensor network with p sensors using a) actual measurements, and b) Bayesian virtual sensors.

in the data space, which is supposed to indicate damage. If the first PC scores of the residuals are not normally distributed and the distribution is unknown, a generalized extreme value distribution can be used regardless of the data distribution [53]. The scores are divided into subgroups (of size $n = 100$) and the subgroup minima and maxima are stored. Extreme value distributions are identified for both the subgroup minima and maxima of the in-control samples (training data). The control limits are computed to these distributions by choosing the probability of exceedance (here 0.001). The extreme values are plotted on a control chart [54] to see if the test samples exceed the control limits thus indicating damage.

The increased sensitivity to damage when using Bayesian virtual sensing instead of the raw measurements can be explained by Eq. (21). If no noise reduction is applied, $\mathbf{y}_u$ is the actual noisy measurement from which a less noisy estimate $E(\mathbf{y}_u|\mathbf{y}_v)$ is subtracted. The noise of the original data thus remains in the residual. On the other hand, when applying Bayesian virtual sensing, $\mathbf{y}_u$ will have less noise than the actual measurement, and subtracting $E(\mathbf{y}_u|\mathbf{y}_v)$ will result in a less noisy residual, which is beneficial to damage detection.

4. Numerical example

The proposed damage detection algorithm in the time domain was studied with a finite element model of a stiffened bridge deck (Fig. 3 and Fig. 4a). The performance of damage detection whether using the actual measurements or virtual sensors was compared.

The length of the bridge was 30 m and the width was 11 m. The slab was stiffened with four girders and three lateral plates. The slab was made of concrete with a Young's modulus of $E = 40$ GPa (at temperature $T = 0$ °C), Poisson ratio of $v = 0.15$, density of $\rho = 2500$ kg m^{-3}, and thickness of 250 mm. The stiffeners were made of steel ($E = 207$ GPa, $v = 0.30$, $\rho = 7850$ kg m^{-3}). The web of the girders had a thickness of $t = 16$ mm and a height of $h = 1.4$ m. The flanges had a thickness of $t = 50$ mm and a width of $b = 700$ mm. The lateral plates were 1.4 m high and 30 mm thick.

Four-node discrete Kirchhoff quadrilateral shell elements were used with a diagonal mass matrix. The bottom flanges were simply supported at both ends of the bridge, whereas the longitudinal displacements were fixed only at one end of the bridge. The corners of the concrete slab were supported both in the lateral and vertical directions.

The Young's modulus of the concrete slab varied with temperature. The ends of the bridge were at random temperatures between -20 °C and $+40$ °C. The spatial distribution of the temperature was assumed linearly varying along the length of the bridge, while along the width it was assumed constant. The relationship between the temperature and the Young's modulus
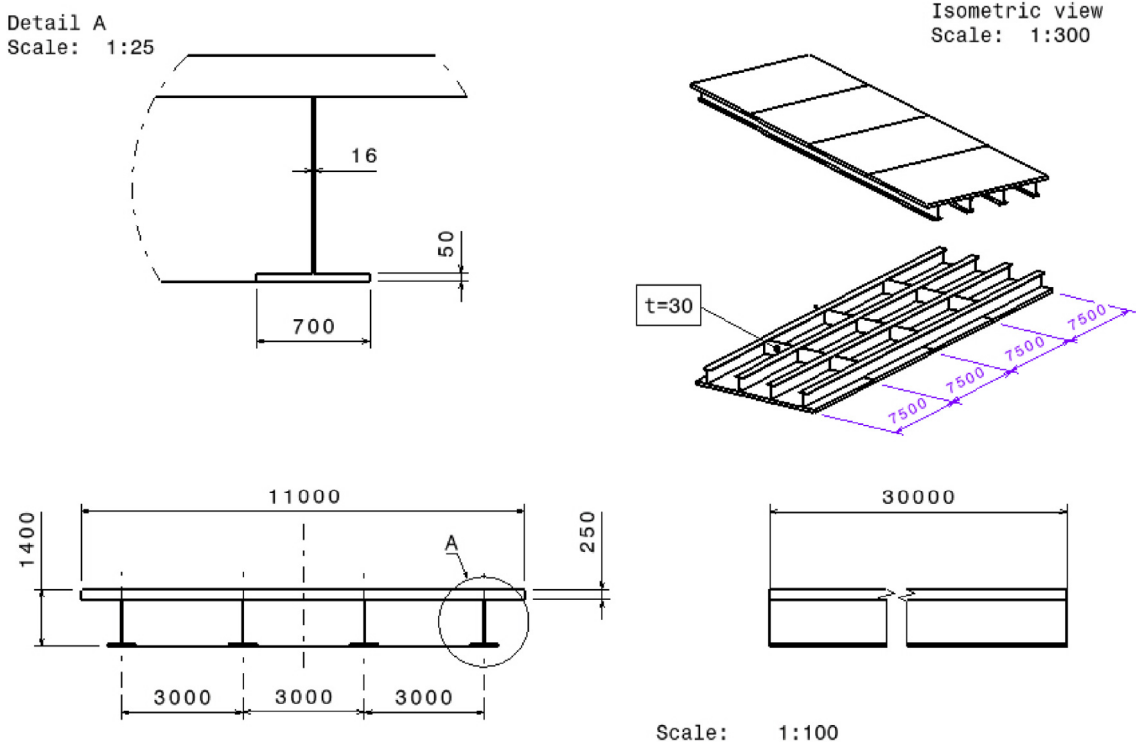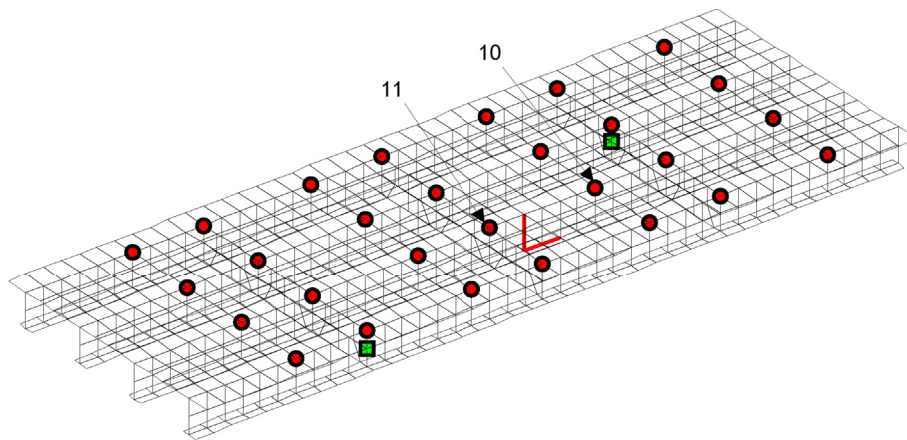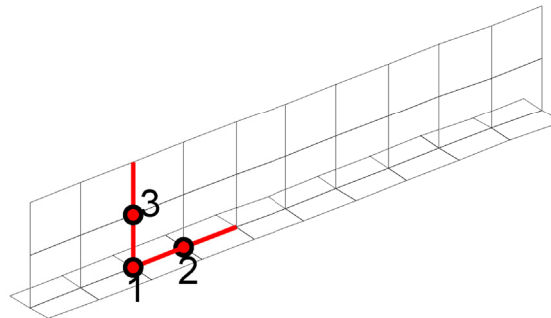

Fig. 3. The main dimensions (mm) of the bridge deck.

(a)

(b)

Fig. 4. a) Finite element model representing the actual structure. The 28 sensor positions are shown with red circles and the two excitation points with green squares. Damage is shown with red lines. Two sensors nearest to the crack are also indicated. b) A detail of the girder with damage. The crack is shown with red lines and the numbers indicate the order in which the connecting nodes separated to form an increasing crack size. The flange remained intact. (For interpretation of the references to colour in this figure legend, the reader is referred to the Web version of this article.)

was stepwise linear as shown in Fig. 5. There was thus an infinite number of possible distributions of the Young's modulus in the slab. Notice that the temperature or the Young's modulus were not measured, but they were considered latent variables.

Two independent random loads were applied in the vertical direction at nodes plotted with green squares in Fig. 4a. The excitation was low-pass filtered below 8.33 Hz. The standard deviation of either load was random between 30 N and 200 N. The excitation was not measured.

The response was computed with modal superposition using the first seven modes. The analysis period was 2 s with a sampling frequency of 500 Hz. One measurement period then included 1001 samples from each sensor.

Vertical accelerations were measured at 28 points shown in Fig. 4a. An equal amount of noise was added to the signals, so that the mean signal-to-noise ratio was approximately SNR = 48 dB. The standard deviation of the noise was $\sigma_w = 3 \cdot 10^{-6}$ m s^{-2}, which was assumed to be known.

Fifty measurements were made from the undamaged structure under random environmental conditions. Damage was a crack that was simulated by removing contact between elements at selected nodes. The damage location is plotted in red in Fig. 4a. Three different crack configurations were modelled with an increasing severity by removing contact between the
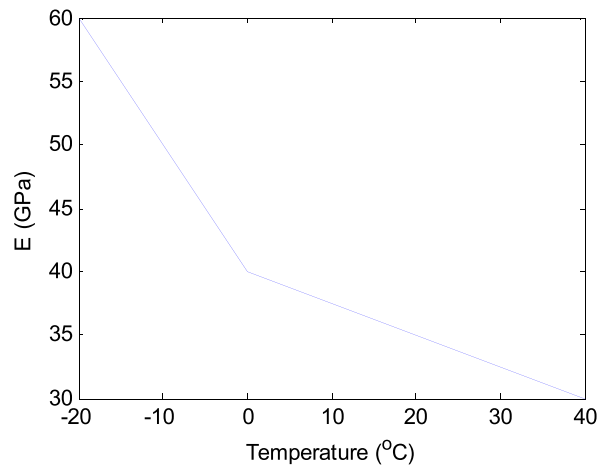
Fig. 5. The effect of temperature on the Young's modulus of the concrete.

elements at one, two, or three nodes, respectively. The nodes are shown in the detailed plot in Fig. 4b showing the order in which the nodes were separated. Each damage scenario was monitored with three measurements under random environmental and operational conditions. As a result, the last nine measurements were from a damaged structure. Notice that the crack was in the web and in the weld between the web and the flange making damage detection quite challenging, because the flanges remained intact.

Fig. 6 shows the first seven natural frequencies in each 59 measurements. The variability due to environmental variation is clearly seen. Visually, there are no clear changes in natural frequencies due to damage. The red circles show an additional natural frequency due to damage corresponding to the lateral flapping of the web at the crack. This had no effect on the data analysis, which is one advantage of the time domain approach.

The training data were the first 40 measurements. They were also used to design the control charts. The test data were the last 19 measurements, from which the last nine were from the damaged structure. The minima and maxima of the first principal component scores of the residuals, Eq. (21), were plotted on the extreme value statistics (EVS) control chart using subgroups of size 100 [55].

The objective was not to create a very detailed finite element model. Instead, the purpose was to investigate the performance of the Bayesian virtual sensors to damage detection compared to the corresponding hardware. For the modelled damage, the noise level was deliberately chosen so that the comparison could be easily made. Nevertheless, the selected noise level would give an indication of the possible crack size that can be detected with the actual hardware. An open crack was
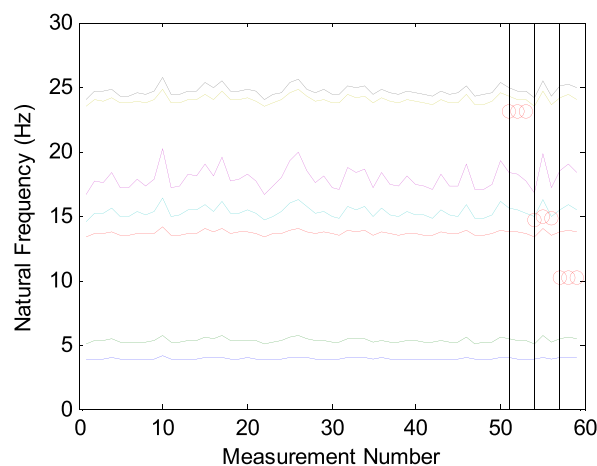

Fig. 6. The first natural frequencies indicating the influences of the environmental variables and damage. The data before the leftmost vertical line were from the undamaged structure, and the vertical lines indicate the three damage levels with an increasing severity. The red circles are additional natural frequencies due to damage. (For interpretation of the references to colour in this figure legend, the reader is referred to the Web version of this article.)

modelled instead of a breathing crack, because it was shown in an earlier study that a breathing crack may be easier to detect than an open crack due to resulting non-linear effects [56].

The empirical Bayesian virtual sensors were estimated using the physically measured 28 accelerations. Fig. 7 shows a detail of the acceleration of sensor 10. Three curves are shown: the noiseless data (red dots), the actual noisy measurement (black), and the Bayesian virtual sensor (blue crosses). A larger noise level was used to make a visual comparison possible. For the actual noise level, the standard deviation of the noise in sensor 10 is plotted in Fig. 8 both for the hardware (red dashed line) and the corresponding Bayesian virtual sensor (blue solid line). It can be seen that the Bayesian virtual sensor was more accurate than the actual hardware. The standard deviation of the noise was decreased to one third on average. This noise reduction property was utilized in damage detection as shown next.

EVS control charts for damage detection are shown in Fig. 9. The left chart (Fig. 9a) was plotted using the actual measurements indicating no damage, whereas the chart in the right (Fig. 9b) that was plotted using the virtual sensors was able to detect damage levels 2 and 3. It should be noted that the measurement error (noise) was small indicating that high-quality sensors may be required to detect damage of this type and size. Nevertheless, with Bayesian virtual sensors it was possible to detect damage earlier than if using the physical hardware. Notice also that no false alarms occurred in either case.

Damage was assumed to locate in the vicinity of the sensor u with the largest Mahalanobis distance (MD) [52] of the residual, Eq. (21). The MDs of the residuals for each sensor are plotted in Fig. 10. Damage was localized to sensor 10 that was the next sensor to the right from the actual damage location and above the same girder (Fig. 4b). The closest sensor from the crack was sensor 11, which also showed a large residual. It was located above the intersection of the longitudinal and lateral stiffeners.
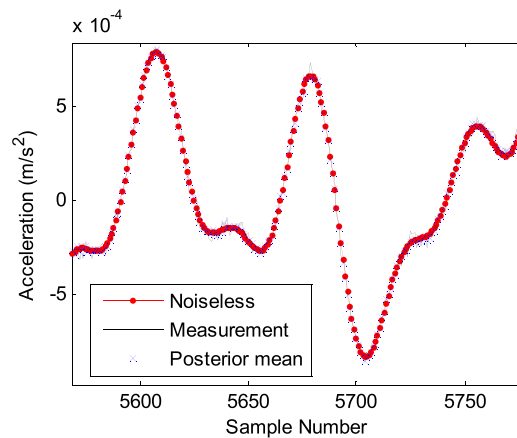

Fig. 7. Time history of sensor 10. Red dots: true (noiseless) data. Black: actual noisy measurement. Blue crosses: Bayesian virtual sensor. A larger measurement error ($\sigma_w = 3 \cdot 10^{-5}$ m s^{-2}) was used to enable visual comparison. (For interpretation of the references to colour in this figure legend, the reader is referred to the Web version of this article.)
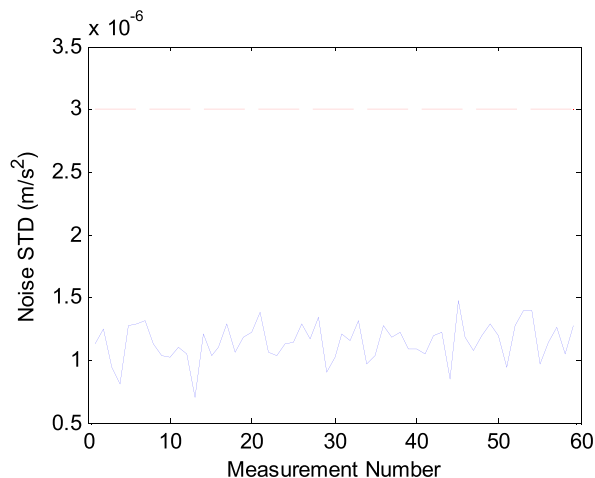

Fig. 8. Standard deviation of noise in the actual sensor 10 (red dashed line) in each measurement, and the noise of the Bayesian estimate (blue solid line). (For interpretation of the references to colour in this figure legend, the reader is referred to the Web version of this article.)
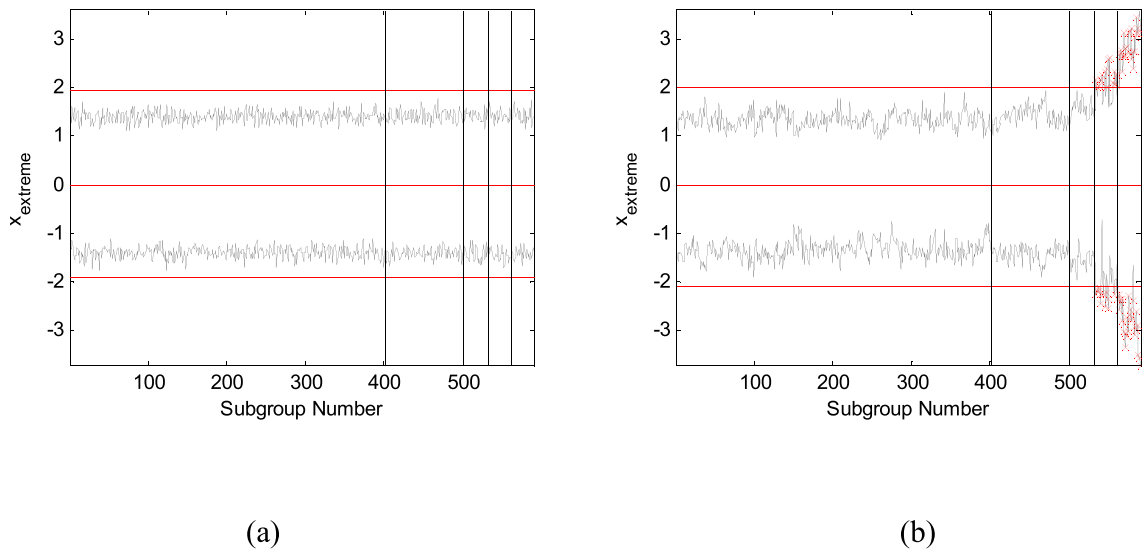
(a) (b)

Fig. 9. EVS control charts using a) the actual measurements and b) the Bayesian virtual sensors. The data before the leftmost vertical line were used as the training data, and the other vertical lines indicate the three damage levels with an increasing severity.
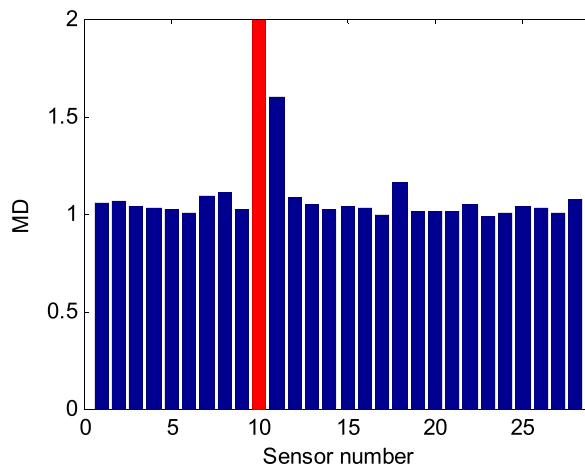

Fig. 10. Damage localization.

The sensor network in this study included 28 accelerometers, which is a large number for practical applications. The very same data were also analysed using a smaller number of sensors and applying virtual sensing. With 14 sensors, the detection performance decreased only little, but with 7−10 sensors, the largest crack could only be detected. This can be explained with the noise reduction capability that depends on the number of sensors.

5. Conclusion

Bayesian virtual sensing was introduced and applied to damage detection. With Bayesian VS it is possible to decrease the measurement error making an early warning more plausible. Virtual sensors were estimated for each measurement individually, so that the dynamics and environmental or operational influences remained, but noise was only decreased. The resulted virtual sensor data then replaced the actual measurements in damage detection. It was shown that the detection performance increased when using Bayesian virtual sensors instead of the actual measurements in the proposed algorithm.

Virtual sensors were estimated at time t, computed from measurements at the same instant. No restrictions were therefore placed on the sampling frequency, which may be useful in some applications. Simultaneous sampling was nevertheless necessary.

Data analysis for damage detection was made in the time domain without a feature extraction process, without knowing the excitation or the environmental or operational variables, and without a mathematical model of the structure.

Environmental and operational effects were eliminated using the correlation between the virtual sensors. The training data were used to build a correlation model of the undamaged structure under different environmental or operational conditions. The training data were used to estimate one sensor in turn using the remaining virtual sensors in the network. The residuals were generated by subtracting the conditional mean from the virtual sensor data. Principal component analysis was applied to the residuals and the first PC scores were used to design the extreme value statistics control chart for damage detection with appropriate control limits. Damage was localized to the closest sensor having the largest Mahalanobis distance.

The noise level used in the experiment was quite low, and the results indicated that high-quality sensors may be required to detect the introduced damage. Another study could be made by increasing the crack size gradually to find the smallest detectable crack size using a larger noise level. In addition, other crack locations or damage scenarios could be studied.

The sensor network had 28 accelerometers, which were placed in a 4×7 grid. Optimal sensor placement for damage detection was left for future studies. The measurement error can be further decreased by increasing the number of sensors. The noise reduction rate, however, is not linear but would rapidly decrease similarly to the standard error in a normal averaging process.

An experimental study is necessary to validate the proposed method. There are also several other techniques for damage detection and localization using vibration measurements. As mentioned earlier, damage detection is typically based on damage-sensitive features extracted from the time histories. Therefore, a comparison of the proposed method to other approaches is needed. Actually, a recent study showed that feature-based damage detection had a higher probability of detection (POD) than the proposed method [57]. Benchmark data are important in this regard making it possible to compare algorithms of different research groups. Nevertheless, time-domain data-based damage detection is an interesting alternative having several advantages.

Declaration of competing interest

None.

Acknowledgements

References

[1] C. Boller, F.-K. Chang, Y. Fujino (Eds.), Encyclopedia of Structural Health Monitoring, vol. 1, Wiley, Chichester, UK, 2009.
[2] S. Khatir, S. Tiachacht, C.-L. Thanh, T.Q. Bui, M. Abdel Wahab, Damage assessment in composite laminates using ANN-PSO-IGA and Cornwell indicator, Compos. Struct. 230 (2019) 111509.
[3] S. Khatir, M. Abdel Wahab, Fast simulations for solving fracture mechanics inverse problems using POD-RBF XIGA and Jaya algorithm, Eng. Fract. Mech. 205 (2019) 285–300.
[4] S. Khatir, M. Abdel Wahab, A computational approach for crack identification in plate structures using XFEM, XIGA, PSO and Jaya algorithm, Theor. Appl. Fract. Mech. 103 (2019) 102240.
[5] S. Khatir, K. Dekemele, M. Loccufier, T. Khatir, M. Abdel Wahab, Crack identification method in beam-like structures using changes in experimentally measured frequencies and Particle Swarm Optimization, Compt. Rendus Mec. 346 (Issue 2) (2018) 110–120.
[6] H. Tran-Ngoc, S. Khatir, G. De Roeck, T. Bui-Tien, M. Abdel Wahab, Model updating for Nam O bridge using Particle Swarm optimization algorithm and genetic algorithm, Sensors 18 (12) (2018) 4131.
[7] S. Tiachacht, A. Bouazzouni, S. Khatir, M. Abdel Wahab, A. Behtani, R. Capozucca, Damage assessment in structures using combination of a modified Cornwell indicator and genetic algorithm, Eng. Struct. 177 (2018) 421–430.
[8] S. Khatir, M. Abdel Wahab, D. Boutchicha, T. Khatir, Structural health monitoring using modal strain energy damage indicator coupled with teaching-learning-based optimization algorithm and isogeometric analysis, J. Sound Vib. 448 (2019) 230–246.
[9] H. Tran-Ngoc, S. Khatir, G. De Roeck, T. Bui-Tien, M. Abdel Wahab, An efficient artificial neural network for damage detection in bridges and beam-like structures by improving training parameters using cuckoo search algorithm, Eng. Struct. 199 (2019) 109637.
[10] S.M. Kay, Fundamentals of Statistical Signal Processing. Detection Theory, Prentice-Hall, Upper Saddle River, NJ, 1998.
[11] J. Kullaa, Bayesian virtual sensing in structural dynamics, Mech. Syst. Signal Process. 115 (2019) 497–513.
[12] A. Ray, R. Luck, An introduction to sensor signal validation in redundant measurement systems, IEEE Contr. Syst. Mag. 11 (1991) 44–49.
[13] R. Dunia, S.J. Qin, T.F. Edgar, T.J. McAvoy, Identification of faulty sensors using principal component analysis, AIChE J. 42 (1996) 2797–2812.
[14] R. Dunia, S.J. Qin, Joint diagnosis of process and sensor faults using principal component analysis, Contr. Eng. Pract. 6 (1998) 457–469.
[15] M.I. Friswell, D.J. Inman, Sensor validation of smart structures, J. Intell. Mater. Syst. Struct. 10 (1999) 973–982.
[16] M. Abdelghani, M.I. Friswell, Sensor validation for structural systems with additive sensor faults, Struct. Health Monit. 3 (2004) 265–275.
[17] G. Kerschen, P. De Boe, J.-C. Golinval, K. Worden, Sensor validation using principal component analysis, Smart Mater. Struct. 14 (2005) 36–42.
[18] J. Kullaa, Sensor fault identification and correction in structural health monitoring, in: Proceedings of ISMA2006, International Conference on Noise and Vibration Engineering, Leuven, Belgium, September 18–20, 2006, pp. 873–884.
[19] J. Kullaa, Sensor fault identification and correction in vibration-based multichannel structural health monitoring, in: Proceedings of the 6th International Workshop on Structural Health Monitoring, Stanford, CA, September 11–13, 2007, DEStech, 2007, pp. 606–613.
[20] M. Abdelghani, M.I. Friswell, Sensor validation for structural systems with multiplicative sensor faults, Mech. Syst. Signal Process. 21 (2007) 270–279.
[21] M.R. Hernandez-Garcia, S.F. Masri, Multivariate statistical analysis for detection and identification of faulty sensors using latent variable methods, Adv. Sci. Technol. 56 (2008) 501–507.
[22] J. Kullaa, Three models for sensor validation, in: Proceedings of the 7th International Workshop on Structural Health Monitoring, Stanford, CA, September 9–11, 2009, DEStech, 2009, pp. 529–536.
[23] J. Kullaa, Sensor validation using minimum mean square error estimation, Mech. Syst. Signal Process. 24 (2010) 1444–1457.
[24] J. Kullaa, Detection, identification, and quantification of sensor fault in a sensor network, Mech. Syst. Signal Process. 40 (2013) 208–221.
[25] M.A. Wahab, G. De Roeck, Effect of temperature on dynamic system parameters of a highway bridge, Struct. Eng. Int. 4 (1997) 266–270.
[26] C.R. Farrar, S.W. Doebling, P.J. Cornwell, E.G. Straser, Variability of modal parameters measured on the alamosa canyon bridge, in: Proceedings of IMAC-XV, A Conference on Structural Dynamics, Orlando, Florida, 1997, pp. 257–263.

[27] S. Alampalli, Influence of in-service environment on modal parameters, in: Proceedings of the 16th International Modal Analysis Conference, Santa Barbara, California, 1998, pp. 111−116.

[28] P. Cornwell, C.R. Farrar, S.W. Doebling, H. Sohn, Structural testing series: Part 4. Environmental variability of modal properties, Exp. Tech. 23 (1999) 45−48.

[29] B. Peeters, G. De Roeck, One year monitoring of the Z24 Bridge: environmental influences versus damage effects, in: Proceedings of IMAC-XVIII: A Conference on Structural Dynamics, San Antonio, Texas, February 7−10, 2000, pp. 1570−1576.

[30] R.G. Rohrmann, M. Baessler, S. Said, W. Schmid, W.F. Ruecker, Structural causes of temperature affected modal data of civil structures obtained by long time monitoring, in: Proceedings of IMAC-XVIII: A Conference on Structural Dynamics, San Antonio, Texas, February 7−10, 2000, pp. 1−7.

[31] G.R. Darbre, J. Proulx, The need for system identification techniques using ambient vibration data recorded on large dams, in: Proceedings of the International Conference on Structural System Identification, Kassel, Germany, September 5−7, 2001, pp. 205−213.

[32] J. Kullaa, Elimination of environmental influences from damage-sensitive features in a structural health monitoring system, in: Proceedings of the First European Workshop on Structural Health Monitoring, Paris, France, July 10−12, 2002, DEStech, 2002, pp. 742−749.

[33] Á. Cunha, E. Caetano, C. Moutinho, F. Magalhães, Continuous dynamic monitoring of bridges: different perspectives of application, in: Advanced Materials Research, vol. 745, Trans Tech Publications, 2013, pp. 89−99.

[34] G. Comanducci, F. Magalhães, F. Ubertini, Á. Cunha, On vibration-based damage detection by multivariate statistical techniques: application to a long-span arch bridge, Struct. Health Monit. 15 (2016) 505−524.

[35] W.-H. Hu, S. Thöns, R.G. Rohrmann, S. Said, W. Rücker, Vibration-based structural health monitoring of a wind turbine system. Part II: environmental/operational effects on dynamic properties, Eng. Struct. 89 (2015) 273−290.

[36] G. Manson, Identifying damage sensitive, environment insensitive features for damage detection, in: Proceedings of the Third International Conference on Identification in Engineering Systems, Swansea, 2002, pp. 187−197.

[37] J. Kullaa, Is temperature measurement essential in structural health monitoring?, in: Proceedings of the 4th International Workshop on Structural Health Monitoring, Stanford, CA, September 15−17, 2003 DEStech, 2003, pp. 717−724.

[38] H. Sohn, K. Worden, C.R. Farrar, Statistical damage classification under changing environmental and operational conditions, J. Intell. Mater. Syst. Struct. 13 (2003) 561−574.

[39] J. Kullaa, Latent variable models to eliminate the environmental effects in structural health monitoring, in: Proceedings of the Third European Conference on Structural Control, vol. II, 2004, pp. 55−58. Vienna, Austria, July 12−15.

[40] S. Vanlanduit, E. Parloo, B. Cauberghe, P. Guillaume, P. Verboven, A robust singular value decomposition for damage detection under changing operational conditions and structural uncertainties, J. Sound Vib. 284 (2005) 1033−1050.

[41] A.-M. Yan, G. Kerschen, P. De Boe, J.-C. Golinval, Structural damage diagnosis under varying environmental conditions—Part I: a linear analysis, Mech. Syst. Signal Process. 19 (2005) 847−864.

[42] A.-M. Yan, G. Kerschen, P. De Boe, J.-C. Golinval, Structural damage diagnosis under varying environmental conditions—Part II: local PCA for non-linear cases, Mech. Syst. Signal Process. 19 (2005) 865−880.

[43] J. Kullaa, Removing non-linear environmental influences from structural features, in: Proceedings of the Third European Workshop on Structural Health Monitoring, Granada, Spain, July 5−7, 2006, DEStech, 2006, pp. 635−642.

[44] A.-M. Yan, J.-C. Golinval, Null subspace-based damage detection of structures using vibration measurements, Mech. Syst. Signal Process. 20 (2006) 611−626.

[45] M. Basseville, F. Bourquin, L. Mevel, H. Nasser, F. Treyssède, Merging sensor data from multiple temperature scenarios for vibration-based monitoring of civil structures, in: Proceedings of the Third European Workshop on Structural Health Monitoring, Granada, Spain, July 5−7, 2006, DEStech, 2006, 759−506.

[46] V. Lämsä, J. Kullaa, Nonlinear factor analysis in structural health monitoring to remove environmental effects, in: Proceedings of the 6th International Workshop on Structural Health Monitoring, Stanford, CA, September 11−13, 2007, DEStech, 2007, pp. 1092−1099.

[47] D. Gorinevsky, S.-J. Kim, S. Boyd, G. Gordon, S. Beard, F.-K. Chang, Optimal estimation of accumulating damage trend from series of SHM images, in: Proceedings of the 6th International Workshop on Structural Health Monitoring, Stanford, CA, September 11−13, 2007, DEStech, 2007, pp. 1340−1346.

[48] J. Kullaa, Eliminating environmental *or operational influences in structural health monitoring using the missing data analysis*, J. Intell. Mater. Syst. Struct. 20 (2009) 1381−1390.

[49] E.J. Cross, K. Worden, Q. Chen, Cointegration: a novel approach for the removal of environmental trends in structural health monitoring data, Proceedings of the Royal Society A 467 (2011) 2712−2732.

[50] J. Kullaa, Structural Health Monitoring under Nonlinear Environmental or Operational Influences, Shock and Vibration, 2014.

[51] H.W. Sorenson, Parameter Estimation. Principles and Problems, Marcel Dekker, New York, 1980.

[52] C.M. Bishop, Pattern Recognition and Machine Learning, Springer, New York, 2006.

[53] K. Worden, D. Allen, H. Sohn, C.R. Farrar, Damage detection in mechanical structures using extreme value statistics, in: SPIE Proceedings, vol. 4693, 9th Annual International Symposium on Smart Structures and Materials, San Diego, CA, 2002, pp. 289−299.

[54] D.C. Montgomery, Introduction to Statistical Quality Control, third ed., Wiley, New York, 1997.

[55] J. Kullaa, F. Magalhães, Á. Cunha, Structural health monitoring and damage detection of an arch bridge using a minimum mean square error estimator, Life-Cycle of Engineering Systems: emphasis on Sustainable Civil Infrastructure, in: Proceedings of the Fifth International Symposium on Life-Cycle Civil Engineering (IALCCE 2016). Delft, The Netherlands, 16−19 October 2016, Taylor & Francis, 2016, pp. 777−784.

[56] J. Kullaa, M. Miettinen, Fatigue crack modelling for damage detection, in: Proceedings of the 8th European Workshop on Structural Health Monitoring, Bilbao, Spain, July 5−8, 2016.

[57] J. Kullaa, Comparison of time domain and feature domain damage detection, in: Proceedings of the 8th International Operational Modal Analysis Conference (IOMAC 2019), Copenhagen May 12−14, 2019, pp. 115−126.